

Relationship of microstructure properties to oxygen impurities in nanocrystalline silicon photovoltaic materials

H. Xu, C. Wen, H. Liu, Z. P. Li, and W. Z. Shen

Citation: *J. Appl. Phys.* **113**, 093501 (2013); doi: 10.1063/1.4794353

View online: <http://dx.doi.org/10.1063/1.4794353>

View Table of Contents: <http://jap.aip.org/resource/1/JAPIAU/v113/i9>

Published by the [American Institute of Physics](#).

Related Articles

Violet-blue photoluminescence from Si nanoparticles with zinc-blende structure synthesized by laser ablation in liquids

AIP Advances **3**, 022127 (2013)

Single and multi-particle passive microrheology of low-density fluids using sedimented microspheres

Appl. Phys. Lett. **102**, 074101 (2013)

Dose enhancing behavior of hydrothermally grown Eu-doped SnO₂ nanoparticles

J. Appl. Phys. **113**, 064306 (2013)

Why specific mixed solvent composition leads to appropriate film formation of composite during spin coating?

Appl. Phys. Lett. **102**, 051918 (2013)

Reducing minimum flash ignition energy of Al microparticles by addition of WO₃ nanoparticles

Appl. Phys. Lett. **102**, 043108 (2013)

Additional information on J. Appl. Phys.

Journal Homepage: <http://jap.aip.org/>

Journal Information: http://jap.aip.org/about/about_the_journal

Top downloads: http://jap.aip.org/features/most_downloaded

Information for Authors: <http://jap.aip.org/authors>

ADVERTISEMENT



AIP Advances

Now Indexed in
Thomson Reuters
Databases

Explore AIP's open access journal:

- Rapid publication
- Article-level metrics
- Post-publication rating and commenting

Relationship of microstructure properties to oxygen impurities in nanocrystalline silicon photovoltaic materials

H. Xu, C. Wen, H. Liu, Z. P. Li, and W. Z. Shen^{a)}

Laboratory of Condensed Matter Spectroscopy and Opto-Electronic Physics, Key Laboratory of Artificial Structures and Quantum Control (Ministry of Education), Department of Physics, and Institute of Solar Energy, Shanghai Jiao Tong University, 800 Dong Chuan Road, Shanghai 200240, China

(Received 15 December 2012; accepted 20 February 2013; published online 1 March 2013)

We have fully investigated the correlation of microstructure properties and oxygen impurities in hydrogenated nanocrystalline silicon photovoltaic films. The achievement has been realized through a series of different hydrogen dilution ratio treatment by plasma enhanced chemical vapor deposition system. Raman scattering, x-ray diffraction, and ultraviolet-visible transmission techniques have been employed to characterize the physical structural characterization and to elucidate the structure evolution. The bonding configuration of the oxygen impurities was investigated by x-ray photoelectron spectroscopy and the Si-O stretching mode of infrared-transmission, indicating that the films were well oxidized in SiO₂ form. Based on the consistence between the proposed structure factor and the oxygen content, we have demonstrated that there are two dominant disordered structure regions closely related to the post-oxidation contamination: plate-like configuration and clustered microvoids. © 2013 American Institute of Physics. [<http://dx.doi.org/10.1063/1.4794353>]

I. INTRODUCTION

Over the past decades, hydrogenated nanocrystalline silicon (nc-Si:H) thin films have been intensively studied and its emergence opens up new ways in the next generation of solar cells and thin film transistor applications.^{1,2} Extensive researches have been carried out to find that nc-Si:H films have higher electrical conductivity, better optical absorption, higher photocurrent, higher carrier mobility, and higher doping efficiency than those of amorphous counterpart (a-Si:H).³⁻⁵ However, widespread and large scale manufacturing of this material has been hampered by its inherent structural complexity and inability to directly control the quantum dot dispersion and its size, making it very difficult to accurately predict the optical and electronic properties.

It is well known that nc-Si:H thin films are mixture of various amounts of different structural components, containing isolated Si nanocrystalline grains, amorphous part, and disordered regions (grain boundaries and microvoids). Previous research on nc-Si:H has indicated that the inhomogeneity feature can form localized states within the energy gap.⁶ Defects and grain boundaries play a crucial role in the transport of carries, which is important for most of the practical applications. Furthermore, when nc-Si:H films are used as a window layer or tunnel junction in a-Si based solar cells,⁷ incorporation of oxygen into the nc-Si:H films can lower the optical absorption.⁸ It has been found that nc-Si:H is more sensitive to oxygen impurities than a-Si:H because oxygen can form weak donors in nc-Si:H materials, which raises the Fermi level toward the conduction band.⁹ For the fabrication of highly integrated devices, one of the major difficulties is the oxide formation at the outermost surface of films. Deeper insight into the correlation between the

inhomogeneity structure features and the oxygen impurities is thus of great importance for the improvement of nc-Si:H based thin film solar cell performance.

Since H species have played a key role in affecting radicals during the film growth and nucleation process, the H dilution profiling has been chosen in this work to control the structure evolution. We have performed a detailed structural and optical investigation to analyze the change of the structure features and also to demonstrate the film growth mechanism. The x-ray photoelectron spectroscopy (XPS) spectra were employed to understand the bonding configuration of surface oxygen. The detailed structure evolution analysis and infrared (IR) Si-H stretching mode investigation have been used to figure out the oxygen incorporation mechanism in nc-Si:H photovoltaic films.

II. EXPERIMENTS

The nc-Si:H thin films were grown on both glass (Corning 7059) and double side polished intrinsic single crystalline silicon (c-Si) (100) substrates at temperature of 250 °C by radio frequency (13.56 MHz) plasma enhanced chemical vapor deposition (PECVD) with silane (SiH₄) and hydrogen (H₂). The total reactive gas flow rate was 120 sccm and the chamber pressure remained at 150 Pa. The substrates were cleaned prior to deposition by immersion consecutively in ultrasonic baths of deionised water for 30 min and then dipped in buffered hydrofluoric acid to remove any native silicon oxidation layer on the surface. The hydrogen dilution ratio R_H [H₂/(H₂ + SiH₄)] was varied from 97.5% to 99.2%. The detailed parameters of these samples have been summarized in Table I.

The x-ray diffraction (XRD) measurements were performed at room temperature on a Goniometer Ultima IV instrument in the standard θ - 2θ configuration with a Cu K α radiation (40 kV, 30 mA). The micro-Raman spectra were

^{a)}Author to whom correspondence should be addressed. Electronic mail: wzshen@sjtu.edu.cn.

TABLE I. Parameters of the nc-Si:H films. R_H is the hydrogen dilution ratio $H_2/(H_2+SiH_4)$ in the film growth, d the average grain size derived from XRD (111) peaks, X_C the crystalline fraction calculated from Raman spectra, n_∞ the refractive index in the long wavelength limit deduced from optical transmission spectra, C_O the bonded oxygen content studies from IR-absorption spectra, I_{1080} and I_{Si-O} the integrated area of the peak at 1080 cm^{-1} and the integrated area of the stretching mode, respectively, R_d the growth rate obtained from step profilometer measurements, and Γ the disorder structure factor from the definition of Eq. (2).

R_H (%)	D (nm)	X_C (%)	n_∞	C_O (at.%)	I_{1080} (cm^{-2})	I_{Si-O} (cm^{-2})	R_d ($\text{\AA}/\text{s}$)	Γ
97.5	8.6	76.83	2.980	5.73	2601	5056	0.2895	0.3815
98.0	7.3	75.41	2.768	8.39	31037	43562	0.2583	0.5332
98.2	6.3	73.15	2.744	8.80	120133	185772	0.2540	0.5678
98.6	5.8	72.07	2.663	10.92	158037	217296	0.1966	0.7478
98.8	5.5	74.69	2.650	9.34	126264	194661	0.1830	0.5476
99.0	5.7	74.91	2.625	6.16	67670	114921	0.1806	0.4736
99.2	6.1	75.72	2.541	3.33	36411	53147	0.1778	0.3715

performed at room temperature on a JobinYvon LabRam HR800 UV micro-Raman spectrometer in backscattering configuration mode using an Ar ion laser at a wavelength of 514.5 nm. The laser power density is $1\text{ mW}/\text{mm}^2$ to avoid any beam-induced crystallization. The optical transmission measurements were performed in the region of 300–1000 nm by means of a double-beam ultraviolet-visible-near infrared spectrometer (PerkinElmer UV Lambda 35). Moreover, the thicknesses of the films were measured by a Dektak 6M profilometer.

The hydrogen bonding configuration and oxygen content within the thin films were measured by IR-transmission spectra from 400 to 4000 cm^{-1} under a Nicolet Nexus 870 Fourier transform infrared spectrometer. The XPS was used to study the silicon core energy level of the nc-Si:H. All the spectra obtained with an electron takeoff angle of 90° using an Al $K\alpha$ source monochromatic x-ray radiation. The Kratos charge neutralizer system was used on all the samples to compensate the charging effect of the sample surface. The narrow scan of spectra was collected at high resolution mode with pass energy 20 eV. The bonding energy was calibrated to the C1s emission (284.8 eV) arising from surface contamination. The background from each spectrum was subtracted using a Shirley-type background to remove most of the extrinsic loss structure. It should be noted that we used glass substrates for measurements of XRD, Raman scattering, and optical transmission, and c-Si substrates for IR-transmission and XPS. The influence of different substrates on the film microstructure¹⁰ can be neglected since the lattice strain between the incubation layers and the substrates has little effects on crystallinity under these rather thick nc-Si:H films ($>500\text{ nm}$).

III. RESULTS AND DISCUSSION

A. Film characterization

The grain size of the nc-Si:H films has been obtained from XRD measurements. Figure 1(a) presents a typical XRD pattern of our samples. Peaks of XRD corresponding to (111), (220), and (311) planes are located at $2\theta \sim 28^\circ$, $\sim 47^\circ$, and $\sim 56^\circ$, respectively. The presence of large broadening of (111) and (220) c-Si peaks gives the indication of silicon nanocrystalline phase appeared in the film. The average grain size (d)

in (111) direction can be determined from the well-known Scherrer formula,¹¹ which is shown in Figure 1(b). It can be clearly observed that with the increase of the R_H up to 98.8%, the grain size has significantly decreased from the maximum value of 8.6 nm to 5.5 nm in nc-Si:H thin films. Further increase of hydrogen dilution from 98.8% to 99.2% only leads to slight increment of the grain size. As we will discuss below, this can be in principle due to the depletion of deposited radical SiH_x molecules by the hydrogen flux.

The film crystallinity can be obtained from the Raman spectroscopy in the $400\text{--}600\text{ cm}^{-1}$ region. Figure 1(c) shows the typical experimental results corresponding to the sample $R_H = 98.6\%$. The spectra were deconvoluted into three satellite spectra: a broad Gaussian distribution around 480 cm^{-1} which attributes to the transverse optical (TO_1) mode of amorphous silicon; a Lorentzian peak near 520 cm^{-1} which belongs to the asymmetric TO_2 vibrational mode of crystalline silicon,¹² and the intermediate mode of crystal-like phase at grain boundaries around 506 cm^{-1} .¹³ The crystalline volume fraction (X_C) in nc-Si:H can be estimated from the relation:

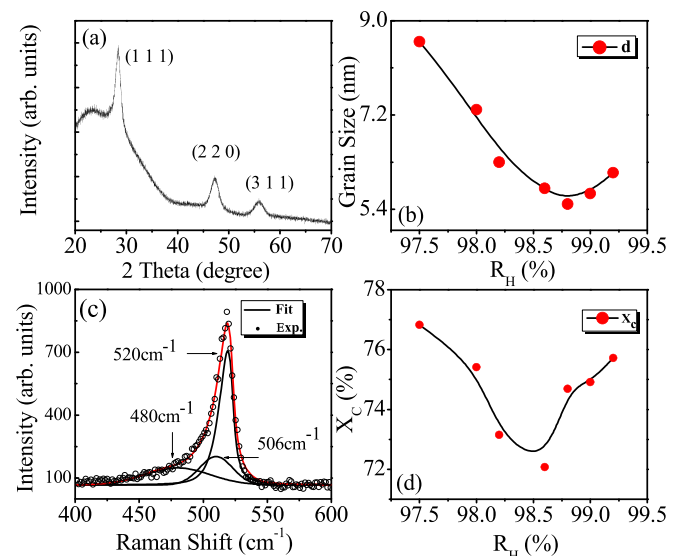


FIG. 1. Typical structural results obtained from the nc-Si:H thin films. (a) Experimental XRD spectrum showing diffraction peaks of (111), (220), and (311) under $R_H = 98.2\%$, (b) average grain sizes, (c) Raman spectrum under $R_H = 98.6\%$, and (d) crystalline volume fractions within the films under different R_H . Solid lines in (b) and (d) are a guide to the eye.

$X_C = (I_A + I_{GB}) / (I_C + I_{GB} + I_A)$, where I_A , I_{GB} , and I_C are the integrated intensity of the peak observed at 480, 506, and 520 cm^{-1} , respectively. We plot in Figure 1(d) the crystalline volume fraction as a function of hydrogen dilution ratio R_H . Similar to XRD, Raman spectra also give us the average information about X_C over the laser detection depth. According to the surface model¹⁴ and growth zone model,¹⁵ the increased hydrogen dilution ratio will be followed by the increase of X_C . We notice that X_C does increase with the R_H over 98.6%; however, X_C decreases with R_H when it is below 98.6%, which cannot be fully explained by those models. Hence, additional discussion is necessary to explain the film growth mechanism to fully understand the structure characterization, which will be presented below from the hydrogen ion bombardment effects.¹⁶

The above-described structural analysis was complemented by optical transmission measurements. Figure 2(a) displays the experimental optical transmission spectrum for the sample $R_H = 98.2\%$ and its fitting results using the envelope method,¹⁷ from which the refractive index n_∞ is yielded by applying the equation: $n(\lambda) = n_\infty + A_n / \lambda^2$, with A_n a fitting parameter. In the meanwhile, the film thickness derived from the envelop fitting is found to be in good agreement with that from direct step profilometer measurements. To further understand the film porosity, nc-Si:H is considered to be a three-phase material with nanocrystallites embedded in amorphous tissues and voids also existed in the films. The triphasic constituents of the nc-Si:H thin films, i.e., the volume fractions of P_C (crystalline Si), P_A (amorphous silicon), and P_V (voids filled with air), can be achieved in terms of Bruggeman's effective media approximation¹⁸ and n_∞ obtained from the optical transmission measurements.

We have also illustrated in the inset of Figure 2(a) the optical gap E_g deduced from the measured absorption spectrum by Tauc plot of using linear extrapolation method,¹⁹ and presented in Figure 2(b) the variation of the deduced values P_V and E_g with R_H . It is clear that a persistent widening of E_g and an increasing P_V can be observed with the increment of R_H . Usually, as more hydrogen is presented in the growing surface, the passivation of dangling bonds with hydrogen atoms will become more evident, greatly reducing the localized defect states and leading to a consistent variation in the density of band tail states.²⁰ Besides, more microvoids formed during the plasma bombardment can also cause a higher value

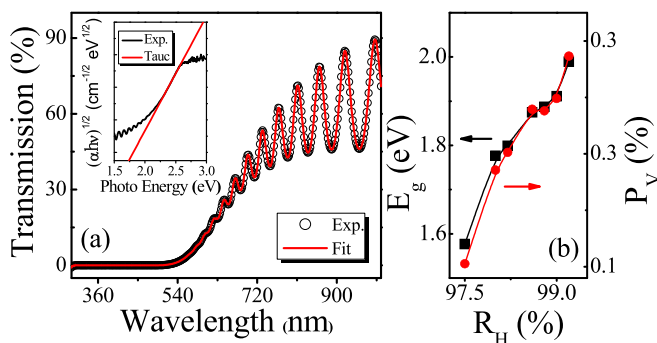


FIG. 2. (a) Experimental (open circles) and fitted (solid curve) transmission spectra with Tauc-plot shown in the inset under $R_H = 98.2\%$. (b) Energy band gap and void volume fraction as a function of hydrogen dilution R_H .

of E_g compared to that in standard a-Si:H (50 meV approximately).²¹ Therefore, it is plausible to assume that there are different bonding configurations and structure features responsible for the observed results in Figures 1 and 2.

Finally, we have performed room-temperature IR-transmission measurements to obtain the oxygen contents in these films. Figure 3(a) shows the IR-absorption spectra of the samples prepared under different R_H , in which major absorption peaks appear at around 630 cm^{-1} (Si-H rocking-wagging mode), 880 cm^{-1} (Si-H bending mode), 1030 cm^{-1} (Si-O stretching mode), and 2090 cm^{-1} (Si-H stretching mode).²² In the calculation of the absorption coefficient, the transmittances are normalized to eliminate the interference fringes due to the small index of refraction difference between the c-Si substrate and the films. The bonded-oxygen content C_O can be yielded by numerical integration of peak around $1000\text{-}1200 \text{ cm}^{-1}$, which is related to the Si-O-Si stretching mode

$$C_O(\text{at.}\%) = \frac{A_W}{N_{Si}} \int_{\nu/w} \frac{\alpha(\nu)}{\nu} d\nu, \quad (1)$$

where $\alpha(\nu)$ represents the absorption coefficient of the film at the wavenumber ν , $N_{Si} = 5 \times 10^{22} \text{ cm}^{-3}$ the atomic density of pure silicon, and the proportionality constant A_W is fixed to $2.8 \times 10^{19} \text{ cm}^{-2}$. The bonded hydrogen content C_H can also be calculated from Si-H rocking mode at around 630 cm^{-1} with A_W being set to $2.1 \times 10^{19} \text{ cm}^{-2}$.²³ The deduced C_O values for all these nc-Si:H films have been listed in Table I.

B. Bonding configurations

Since the oxygen content varies with different microstructures under various R_H values, it can be deduced here that the microstructure characteristics can effectively influence the oxygen impurities in the films, as shown in Figure 3(a). Researchers have the conclusion that most of the oxygen incorporated into the films through postoxidation.²⁴ Our films $R_H = 97.5\%$ and 98.0% were tested by IR-transmission after being exposed to the air for three days, showing the oxygen concentration of about 1.76% and 0.27%, respectively.

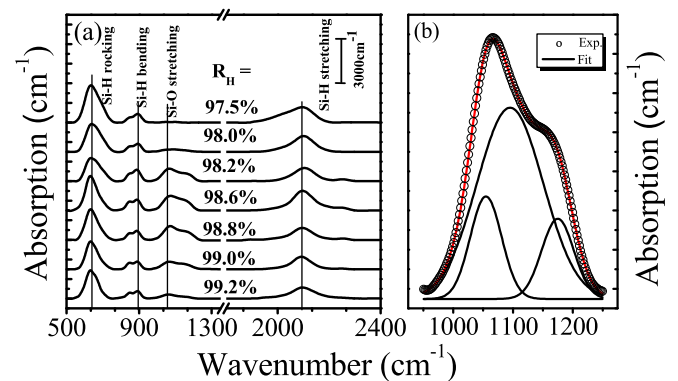


FIG. 3. (a) IR-absorption spectra of the nc-Si:H thin films prepared under different hydrogen dilution as marked; the spectra are shifted for clarity. (b) IR-absorption spectrum of Si-O stretching of the thin film under $R_H = 98.2\%$. The total curve represents the fit with three Gaussian shaped stretching modes.

While we tested the same batch one month later, we found that there exists a big difference in oxygen content (1.76%, 0.27% increased to 8.39%, 5.73%, respectively), which is consistent with previous report.²⁵ However, there is still lack of a convincing explanation on the detailed processes.

Direct bonding configurations of the oxygen impurities in nc-Si:H thin films were investigated by IR-transmission and XPS measurements. The typical oxygen related absorption modes have been demonstrated by the Si-O-Si stretching band spectra in Figure 3(a), which was fitted by three Gaussian curves as shown in Figure 3(b). The lowest frequency peak around 1030 cm^{-1} corresponds to the stretching mode of Si-O-Si configuration, in which Si atoms were in turn back bonded to the other oxygen atoms. The middle one around 1080 cm^{-1} belongs to the Si-O-Si stretching vibration in SiO_2 , and the component around 1150 cm^{-1} comes from the out-of-phase oxygen motion associated with an $\text{Si}(\text{O})_4$ configuration.²⁶ It was observed that the peak at 1080 cm^{-1} was significantly stronger than the peaks at 1030 and 1150 cm^{-1} for the sample $R_H = 98.2\%$, which indicates the preferential oxidation form like the Si-O-Si in SiO_2 bulk. Besides, as shown in Figure 3(a), the integrated area of the Si-O stretching mode gradually increases to its biggest value of when increasing R_H up to 98.6% , while further increasing R_H , the integrated area comes to exhibit a downshift. As also listed in Table I, the integrated area of the peak at 1080 cm^{-1} , referred as I_{1080} , has a similar variation with that of the integrated area of the stretching mode $I_{\text{Si-O}}$, revealing that SiO_2 appears to be the most predominant basic configurations for all the samples.

We have further employed the XPS measurements to accurately investigate the Si/O surface interaction. Figure 4(a) displays the high-resolution Si 2p, O 1s photoelectron emission peaks taken at the surfaces of these films. The high resolution Si 2p spin orbital splitting of 0.6 eV was observed with a defined intensity ratio of Si $2p_{1/2}$ and Si $2p_{3/2}$ of 1:2. It is clear from the evolution of the Si 2p spectral region that the peak position in most cases downshifts towards the lowest banding energy 99.35 eV upon R_H increasing up to 98.6% , which almost approaches to the value for bulk Si (99.7 eV). When R_H further increases to 99.2% , the peak position shifts

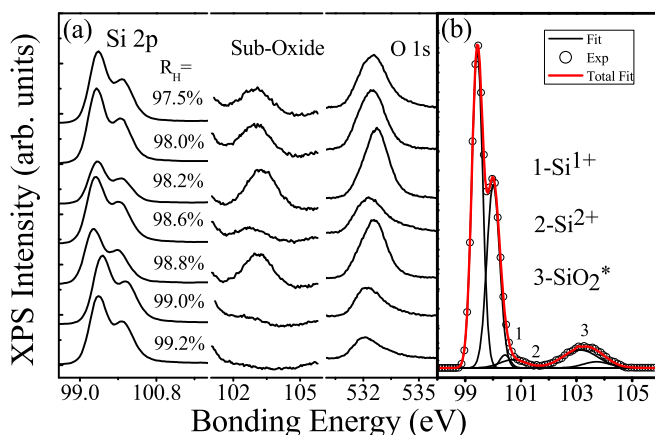


FIG. 4. (a) Si 2p, sub-oxide and O 1s XPS spectra for the different hydrogen dilution R_H . (b) Typical XPS Si 2p spectrum of the nc-Si:H thin film under $R_H = 98.2\%$. The splitting of 0.6 eV is shown with all the intermediate oxidation states.

toward the higher value 99.439 eV . This broad Si 2p peak shift may be due to the electronegativity of oxygen, so the Si 2p peak in oxidized silicon has a higher binding energy in comparison to that in less oxidized films. Here, note that there is a seemingly random change in Si $2p_{3/2}$ emission. Considering that the bonding energy of Si-H_x is very close to the Si 2p core level as well as the charge transfer effects,²⁷ bonded hydrogen can attract the positive charge located on Si core level causing a shift of Si core level toward a high binding energy of broadening the Si 2p core level peak. However, it is difficult to differentiate between the influences of suboxides from the Si-H bonding in the bulk,²⁴ which complicated detailed interpretation of the peak shift of our spectra. In the O 1s XPS spectra, the peak intensity shows a random variation, according to the charge transfer model, such a shift is expected to be due to the change of the Fermi level.

Figure 4(b) shows a representative high-resolution Si 2p spectrum for understanding the suboxide on the film surface. All energy level fitting was based on the synchrotron work of Himpfel *et al.*²⁸ and Niwano *et al.*²⁹ The decomposition of the measured spectra into fitting components corresponds to various Si bonding states. For the as-fabricated nc-Si:H materials, the Si 2p region has been routinely fit to Si $2p_{1/2}$ and Si $2p_{3/2}$ partner lines for Si^{4+} , Si^0 , and intermediate states such as Si^{1+} (Si_2O), Si^{2+} (SiO), and Si^{3+} (Si_2O_3). Additional component of silicon oxide was referred as SiO_2^* , which is assigned to be the regular crystalline like phase produced at the interface of SiO_2 -Si. This part mainly comes from the lattice mismatch of the oxide and single crystal Si (Ref. 29) with its peak located at a binding energy 0.35 eV lower than SiO_2 . From the above data analysis, it can be confirmed that Si^{3+} did not exist in the sample, while the existence of Si^{1+} and Si^{2+} species are supported by the XPS observation. Moreover, we can notice that the nc-Si:H surface was well passivated with SiO_2 , which is consistent with our IR-transmission results. In contrast, suboxide spectra of $R_H = 99.0\%$ and 99.2% exhibit very weak SiO_2 peak as illustrated in Figure 4(a), demonstrating that high R_H hydrogen effectively limits the intermediate oxide formation by passivation at the near surface. Finally, the spectrum of $R_H = 98.2\%$ exhibits the highest peak intensity of SiO_2 while the oxygen content in the bulk is not the highest. This may be related to the surface smoothness at an atomic level of the sample, i.e., a rough surface of the silicon material produces more intermediate oxidation states.²⁸

C. Structure evolution and mechanism of oxidation

To fully understand the relation between the microstructure properties and the oxidation effects, it is quite necessary to investigate the structure evolution. The nanocrystalline silicon growth resulted from a complex synergy between surface and bulk reactions of impinging SiH_x radicals, atomic hydrogen, and ion species.^{30,31} As we can see from Table I, the deposition rate R_d decreased monotonously from 0.289 to 0.177 A/s as R_H increased from 97.5% to 99.2% . This variation of R_d closely depended on the two simultaneous processes of the film growth: the forming radicals and the etching of deposition portion. On one hand, with the increase of R_H ,

the gas density of SiH_4 on the deposited layer decreased as the total gas flow was fixed at 120 sccm, which resulted in the decreasing concentration of the deposition precursor SiH_x ($x \leq 3$). On the other hand, more hydrogen ions were introduced into the deposition system with the increasing R_H , which led to excessive etching on the weak Si-Si bonds. As a result, the value of R_d decreased.

Furthermore, ion bombardment growth mechanism¹⁶ can provide a satisfactory explanation for the experimental XRD and Raman results in Figure 1. As the nc-Si:H films were deposited at a high RF power (of 60 W) and deposition area of $12.5 \times 12.5 \text{ cm}^2$, the ion bombardment effect should be taken into account. In the bulk layer, the bombardment by hydrogen ion became more evident with increasing R_H from 97.5% to 98.6%. The film growth would undergo the process that hydrogen ions impinged the radicals SiH_x at the weak bonding region, which reduced the surface diffusion length of the film precursors (SiH_x) and more microvoids were created in the grain boundaries with amorphous components. These subsequently formed microvoids induced larger areas of internal surfaces with dangling bonds and weaker Si-Si bonds in the growing film. Therefore, through H ion implantation, atomic hydrogen diffusion, and relevant chemical reactions, more hydrogen would be bonded to silicon or trapped in these microvoids and grain boundaries region, leading to the shrinking of the grain size d and decrease of the crystalline volume fraction X_c , as observed by the XRD and Raman measurements.

However, when increasing R_H from 98.6% to 99.2%, hydrogen-induced annealing effects³² overcame the ion bombardment induced amorphization. With more atomic H presenting on the growing surface, they penetrated into the subsurface and rearranged the Si-Si network structure by the following processes: (1) saturation of present dangling bonds at the interface between the amorphous and the crystalline region; (2) formation of molecular hydrogen through reaction of adsorbed hydrogen with clustered hydrogen in the subsurface, which was less mobile than the atomic hydrogen; and (3) destruction and perturbation the strained Si-Si bond by H-insertion reaction with the a-Si:H matrix. Subsequent structural relaxation of the Si-Si bonds results in the transformation of the film's structure from amorphous to nanocrystalline. Therefore as a general result, more hydrogen presenting in the plasma could lead to greater probability of crystallization, supported by the observation in Figure 1(d). The reason for the grain size without remarkable change [5.5 to 6.1 nm, see Figure 1(b)] can be attributed to the suppression of the growth by the H ion implantation on the nucleation site, as well as the depletion of radical SiH_x by the hydrogen flux.

To accurately identify the spatial correlation between the hydrogen related microstructures and the oxygen impurities, we can turn to investigate the IR Si-H stretching mode, which was deconvoluted using Gaussian absorption peaks corresponding to different bonding configurations as shown in Figure 5(a). The position of the stretching mode peaks of a hydride in the bulk depends on the unscreened eigenfrequency of the hydride, bulk screening, local hydride density, and possible mutual dipole interactions of the hydrogen incorporation configuration.³³ The low stretching mode

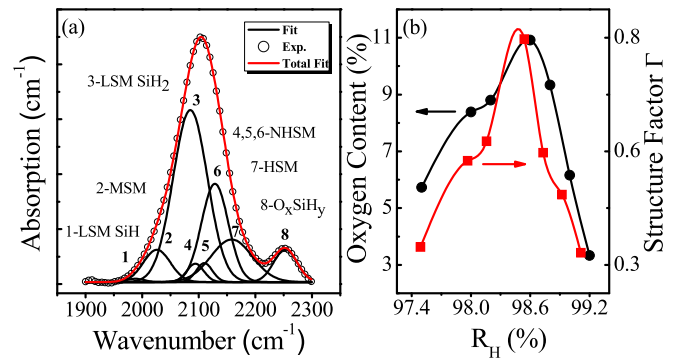


FIG. 5. (a) Typical deconvoluted Si-H stretching mode of the nc-Si:H thin film under $R_H = 98.2\%$. The solid curves are the overall fitting results using eight Gaussian peaks. (b) Correlation between the oxygen content and structure factor as a function of hydrogen dilution R_H .

(LSM, 1980–2010 cm^{-1}) origins from the α -Si:H tissue, which is often in isolated Si-H form in the bulk. The middle stretching mode (MSM, 2024–2041 cm^{-1}) is due to the Si-H stretching vibrations located at the platelet-like configuration of amorphous-crystalline interface with a lot of defect states. The high stretching mode (HSM, 2086–2094 cm^{-1}) represents for Si-H₂ at the internal surface of microvoids,³⁴ which is also related to massive unsaturated dangling bonds. The extreme HSM (EHSM, 2140–2150 cm^{-1}) arises from the trihydrides in the film deposited under high hydrogen dilution condition. Three narrow HSMs (NHSMs at 2097, 2109, and 2137 cm^{-1}) reflect mono-, di-, and trihydrides on the crystalline surface. Furthermore, the stretching mode at $\sim 2250 \text{ cm}^{-1}$ corresponds to the hydride $\text{O}_x\text{Si-H}_y$ vibration with oxygen atoms back bonded to the silicon atoms.³⁵ As a result, the film disorder can be represented by the relative intensities of the MSM and HSM versus the total absorption intensity, and we propose here a factor Γ which is defined as follows:

$$\Gamma = \frac{I_{\text{MSM}} + I_{\text{HSM}}}{I_{\text{LSM}} + I_{\text{MSM}} + I_{\text{HSM}} + I_{\text{NHSM}} + I_{\text{EHSM}}}, \quad (2)$$

where I_{LSM} , I_{MSM} , I_{HSM} , I_{NHSM} , and I_{EHSM} are deconvoluted integrated areas of the IR-absorption curve for Si-H_x, which stand for intensities of absorption from corresponding modes. It is clear from Figure 5(b) that the values of the structure factor at different R_H agree very well with the oxygen content C_O , strongly indicating that oxygen incursion has been originated from these plate-like configuration and clustered microvoids of the disordered regions. Therefore, we can fully understand the spatial correlation between the disordered structure and the oxygen incursion.

First of all, there is a big difference between amorphous tissues and crystalline grain boundaries in the disordered region, that is, the voids formed at the amorphous/crystalline interface are different from microvoids incorporated into bulk amorphous silicon.³⁶ It is widely agreed that isolated hydrides in vacancies contribute to the LSM where hydrogen atom is bonded to silicon in form of monohydrides within small volumes of monovacancy, divacancies, or polyvacancies. This part of the inhomogeneous microvoids distributed in the amorphous tissues does not have an effective pathway for the oxygen bonding, thus the oxygen has less possibility

to bond with the coordinated defects, which can explain the fact that microvoids corresponding to LSM contribute little to the oxygen incorporation. Second, on the grain boundaries silicon hydrides can form platelet-like configuration, created by the insertion of hydrogen into strained Si–Si back bonds during growth, which resulted in MSM peaks of IR-transmission spectra. Our films of highly crystallized nc-Si:H have a high ratio of grain boundaries, providing big opportunity for oxygen to incorporate with the massive dangling bonds along the grain boundaries. In addition, the HSM centered at 2090 cm^{-1} is assigned to clustered hydrogen in mono-, di- or trihydrides at the internal surfaces of voids. Nanosized voids at the interface between amorphous silicon and nanocrystallites, as well as 6-ring like voids configuration³⁷ can provide large space for oxygen habitation.

We can conclude that the nature of the disordered films allowed the oxygen impurities to diffuse along the columnar grain boundaries after being exposed to air. Through electrostatic effects of adsorbents, the oxygen atoms accumulated at large unsaturated internal dangling bonds of the void states led to the inhabitation of the oxygen impurities. Hence, compact structure and well passivated grain boundaries are less susceptible to surface contamination resulted from oxygen. Since the oxygen contaminated surface caused by oxidation can influence the light absorption,⁸ to deposit an amorphous layer on the films of nc-Si:H can be an efficient way to prevent surface contamination from oxygen impurity.

IV. CONCLUSIONS

In summary, we have performed an overall study on the correlation of structure properties and oxidation effects from a series of nc-Si:H films prepared by hydrogen dilution profiling. Raman spectroscopy, XRD, and optical transmission have been employed to elucidate the structure evolution and film growth. XPS measurements indicated that Si^{3+} did not exist in the sample, while the Si^{1+} and Si^{2+} species were existed. Hydrogen limits the intermediate oxide formation by passivating the near surface and reducing the strained bonds at the interface of the disordered region. Crystalline like phase SiO_2 is the highest formation of the oxidation states after the films are exposed to air. The observation of the structure factor corresponding to oxygen spatial dispersion told us that the oxygen incursion has been originated from these plate-like configuration and clustered microvoids. Consequently, compact structure, well bonded grain boundaries, and depositing a quite thin amorphous layer are suitable to reduce the surface oxygen contamination. The present work offers a very valuable understanding of the oxygen incorporation mechanism in the potential good photovoltaic materials.

ACKNOWLEDGMENTS

This work was supported by National Major Basic Research Projects (2012CB934302, 2011AA050502, and 2011AA050518) and Natural Science Foundation of China (11074169, 11174202, and 61234005).

- ¹Y. Xu, Z. Hu, H. Diao, Y. Cai, S. Zhang, X. Zeng, H. Hao, X. Liao, E. Fortunato, and R. Martins, *J. Non-Cryst. Solids* **352**, 1972 (2006).
- ²T. A. Anutgan, M. Anutgan, I. Atilgan, and B. Katircioglu, *J. Non-Cryst. Solids* **356**, 1102 (2010).
- ³X. Y. Chen, W. Z. Shen, H. Chen, R. Zhang, and Y. L. He, *Nanotechnology* **17**, 595 (2006).
- ⁴C. Xu, Z. P. Li, W. Pan, and W. Z. Shen, *Appl. Surf. Sci.* **257**, 8409 (2011).
- ⁵A. M. Funde, N. A. Bakr, D. K. Kamble, R. R. Hawaldar, D. P. Amalnerkar, and S. R. Jadkar, *Sol. Energy Mater. Sol. Cells* **92**, 1217 (2008).
- ⁶J. Kočka, *J. Non-Cryst. Solids* **358**, 1946 (2012).
- ⁷G. Y. Xu, M. Liu, X. S. Wu, Y. L. He, and T. M. Wang, *J. Phys.: Condens. Matter* **11**, 8495 (1999).
- ⁸D. Das, M. Jana, and A. K. Barua, *Sol. Energy Mater. Sol. Cells* **63**, 285 (2000).
- ⁹T. Kilper, W. Beyer, G. Brauer, T. Bronger, R. Carius, M. N. van den Donker, D. Hrunski, A. Lambertz, T. Merdzhanova, A. Muck, B. Rech, W. Reetz, R. Schmitz, U. Zastrow, and A. Gordijn, *J. Appl. Phys.* **105**, 074509 (2009).
- ¹⁰A. Le Donne, S. Binetti, G. Isella, B. Pichaud, M. Texier, M. Acciarri, and S. Pizzini, *Appl. Surf. Sci.* **254**, 2804 (2008).
- ¹¹M. R. Fitzsimmons, J. A. Eastman, M. Müller-Stach, and G. Wallner, *Phys. Rev. B* **44**, 2452 (1991).
- ¹²A. Achiq, R. Rizk, F. Gourbilleau, R. Madelon, B. Garrido, A. Perez-Rodriguez, and J. R. Morante, *J. Appl. Phys.* **83**, 5797 (1998).
- ¹³Z. Iqbal, S. Vepřek, A. P. Webb, and P. Capezuto, *Solid State Commun.* **37**, 993 (1981).
- ¹⁴A. Matsuda, *J. Non-Cryst. Solids* **59–60**, 767 (1983).
- ¹⁵R. A. Street, *Phys. Rev. B* **44**, 10610 (1991).
- ¹⁶B. Kalache, A. I. Kosarev, R. Vanderhaghen, and P. R. I. Cabarrocas, *J. Appl. Phys.* **93**, 1262 (2003).
- ¹⁷H. Chen, M. H. Gullinar, and W. Z. Shen, *J. Cryst. Growth* **260**, 91 (2004).
- ¹⁸E. Fathi, Y. Vygranenko, M. Vieira, and A. Sazonov, *Appl. Surf. Sci.* **257**, 8901 (2011).
- ¹⁹J. Tauc, *Amorphous and Liquid Semiconductors* (Wiley, New York, 1974), Chap. 4.
- ²⁰S. Binetti, M. Acciarri, M. Bollani, L. Fumagalli, H. von Känel, and S. Pizzini, *Thin Solid Films* **487**, 19 (2005).
- ²¹B. Garrido, A. Perez-Rodriguez, J. R. Morante, A. Achiq, F. Gourbilleau, R. Madelon, and R. Rizk, *J. Vac. Sci. Technol. B* **16**, 1851 (1998).
- ²²G. Lucovsky, R. J. Nemanich, and J. C. Knights, *Phys. Rev. B* **19**, 2064 (1979).
- ²³L. Xu, Z. P. Li, C. Wen, and W. Z. Shen, *J. Appl. Phys.* **110**, 064315 (2011).
- ²⁴C. M. Hessel, E. J. Henderson, and J. G. C. Veinot, *J. Phys. Chem. C* **111**, 6956 (2007).
- ²⁵P. G. Hugger, J. D. Cohen, B. J. Yan, G. Z. Yue, J. Yang, and S. Guha, *Appl. Phys. Lett.* **97**, 252103 (2010).
- ²⁶L. He, T. Inokuma, Y. Kurata, and S. Hasegawa, *J. Non-Cryst. Solids* **185**, 249 (1995).
- ²⁷S. Hasegawa, L. He, T. Inokuma, and Y. Kurata, *Phys. Rev. B* **46**, 12478 (1992).
- ²⁸F. J. Himpsel, F. R. McFeely, A. Taleb-Ibrahimi, J. A. Yarmoff, and G. Hollinger, *Phys. Rev. B* **38**, 6084 (1988).
- ²⁹M. Niwano, H. Katakura, Y. Takeda, Y. Takakuwa, N. Miyamoto, A. Hiraiwa, and K. Yagi, *J. Vac. Sci. Technol. A* **9**, 195 (1991).
- ³⁰M. H. Gullinar, H. Chen, W. S. Wei, R. Q. Cui, and W. Z. Shen, *J. Appl. Phys.* **95**, 3961 (2004).
- ³¹P. L. Novikov, A. Le Donne, S. Cereda, L. Miglio, S. Pizzini, S. Binetti, M. Rondanini, C. Cavallotti, D. Chrastina, T. Moiseev, H. von Kanel, G. Isella, and F. Montalenti, *Appl. Phys. Lett.* **94**, 051904 (2009).
- ³²U. Kroll, J. Meier, A. Shah, S. Mikhailov, and J. Weber, *J. Appl. Phys.* **80**, 4971 (1996).
- ³³A. H. M. Smets, T. Matsui, and M. Kondo, *Appl. Phys. Lett.* **92**, 033506 (2008).
- ³⁴T. Anutgan and S. Uysal, *Curr. Appl. Phys.* **13**, 181 (2013).
- ³⁵A. H. M. Smets, T. Matsui, and M. Kondo, *Appl. Phys. Lett.* **92**, 033506 (2008).
- ³⁶J. Müllerová, P. Šutta, G. van Elzakker, M. Zeman, and M. Mikula, *Appl. Surf. Sci.* **254**, 3690 (2008).
- ³⁷A. H. M. Smets and M. C. M. van de Sanden, *Phys. Rev. B* **76**, 073202 (2007).